doi:10.1016/j.jmb.2011.12.057 J. Mol. Biol. (2012) 416, 438–452

Contents lists available at www.sciencedirect.com

Journal of Molecular Biology

journal homepage: http://ees.elsevier.com.jmb

# Metal Binding Dictates Conformation and Function of the Amyloid Precursor Protein (APP) E2 Domain

Sven O. Dahms[1], Ina Könnig[1], Dirk Roeser[1], Karl-Heinz Gührs[2], Magnus C. Mayer[3], Daniela Kaden[3], Gerd Multhaup[3] and Manuel E. Than[1]*

[1]*Protein Crystallography Group, Leibniz Institute for Age Research - Fritz Lipmann Institute (FLI), Beutenbergstr. 11, 07745 Jena, Germany*
[2]*Protein Laboratory, Leibniz Institute for Age Research - Fritz Lipmann Institute (FLI), Beutenbergstr. 11, 07745 Jena, Germany*
[3]*Institute of Chemistry and Biochemistry, Freie Universität Berlin, Thielallee 63, 14195 Berlin, Germany*

*Received 17 November 2011; received in revised form 19 December 2011; accepted 28 December 2011*
Available online 4 January 2012

***Edited by R. Huber***

***Keywords:***
Alzheimer's disease; conformational change; crystal structure; isothermal titration calorimetry (ITC); metal binding

The amyloid precursor protein (APP) and its neurotoxic cleavage product Aβ are key players in the development of Alzheimer's disease and appear essential for neuronal development and cell homeostasis in mammals. Proteolytic processing of APP is influenced by metal ions, protein ligands and its oligomerization state. However, the structural basis and functional mechanism of APP regulation are hitherto largely unknown. Here we identified a metal-dependent molecular switch located within the E2 domain of APP containing four evolutionary highly conserved histidine residues. Three X-ray structures of the metal-bound molecule were solved at 2.6–2.0 Å resolution. Using protein crystallographic and biochemical methods, we characterized this novel high-affinity binding site within the E2 domain that binds competitively to copper and zinc at physiological concentrations. Metal-specific coordination spheres induce large conformational changes and enforce distinct structural states, most likely regulating the physiological function of APP and its processing in Alzheimer's disease.



## Introduction

Deposition of the characteristic senile plaques and neurofibrillary tangles within the brain is a diagnostic hallmark of Alzheimer's disease (AD). Senile plaques accumulate by aggregation of neurotoxic Aβ peptide species derived from the amyloid precursor protein (APP) by sequential proteolysis by β- and γ-secretases. Imbalanced processing or clearance of APP is generally believed to result in AD pathology (reviewed in Refs. 1–3). Interestingly, in AD patients and in APP transgenic mice, the homeostasis of the divalent transition metals copper and zinc is imbalanced. Manipulations of intracellular copper can influence the regulated intramembrane proteolysis of APP as well as the production of Aβ. This implicates a role of APP in metal metabolism and led to the suggestion of metal chelation therapy as a possible anti-AD treatment.[4–6]

Efforts to address the physiological function of APP and its dysfunction in AD are mainly complicated by the multiple domain architecture of the extracellular portion providing multiple functionalities, as well as the largely unknown functional differences and redundancies among the distinct APP family members and their tissue-specific

*Corresponding author. E-mail address: than@fli-leibniz.de.

Abbreviations used: APP, amyloid precursor protein; AD, Alzheimer's disease; CuBD, copper binding domain; MR, molecular replacement; PDB, Protein Data Bank; SAD, single anomalous dispersion; ITC, isothermal titration calorimetry; SPR, surface plasmon resonance; RU, response units; UP, UniProt.

splicing forms (reviewed in Ref. 7). The ectodomain of all APP family members comprises two subdomains of high sequence conservation, the E1 and the E2 domains. Two tightly interacting subdomains constitute the E1 domain,[8] called growth factor-like domain and copper binding domain (CuBD). E1 and E2 are connected by a potentially flexible, less well conserved linker region of unknown function, primarily composed of acidic amino acids (AcD). A second linker of undefined structure, containing the cleavage sites of α- and β-secretases, anchors the whole extracellular part to the single transmembrane helix. Some APP and APLP2 isoforms feature an additional Kunitz-type protease inhibitor domain located between the AcD and E2 (reviewed in Ref. 9). The E1 domain and especially its heparin binding loop mediate homophilic interactions of APP,[10–12] consistent with the heparin-induced dimerization as observed for the isolated E1 domain[8] as well as for sAPPα.[13] The contribution of the E2 domain to the oligomerization of APP is controversially discussed[10,14–17] and might differ between the family members APLP1[18] and APP.[15]

In particular, little is known about possible conformational changes in the E2 domain that may influence its biochemical properties and hence the function of APP in the cellular context. The fold of the E2 domain is highly flexible, indicated by large conformational differences between the available E2 structures. As a result, partially disordered crystals,[19] anisotropic crystals and high overall *B*-factors of the structures[14,16,20] complicated previous X-ray crystallographic studies. In agreement, an NMR study and proteolytic studies showed that only a part of the E2 domain is rigidly folded in solution.[21]

Whether metal-ion-mediated effects in APP physiology relate to metal homeostasis defects in AD pathology is controversially discussed. Originally, the binding sites of copper and zinc ions were identified close to the C-terminus of the APP-E1 domain by peptide mapping.[22,23] Later, His147, His151 and Tyr168 were identified as copper coordination sphere of the CuBD.[24] However, the $Cu^{2+}$ binding site is partially obstructed by the tightly associated growth factor-like domain.[8] Binding of copper to crystals of the isolated CuBD was only observed at high concentrations and in one of the two investigated crystal forms.[24] Considering the low dissociation constant of the full-length protein,[22] an additional yet unknown high-affinity copper binding site in APP can be expected. Similarly, the zinc binding peptide, mapped to amino acids 181–200, showed weaker binding than full-length APP, and potentially distinct coordination sites in APP were discussed.[23]

In order to gain a complete understanding of the structure of the E2 domain that gives rise to its physiologic function, its influence on the entire protein and the development of AD, we analyzed the biochemical properties of this domain especially with respect to its metal binding properties and solved the crystal structure in the presence of different metal ions. We identified a so far unknown competitive metal binding site within the structure of the E2 domain and show a metal-dependent conformational switch regulating the conformation, flexibility and hence the physiological function of APP-E2 and full-length APP.

## Results

### High-resolution X-ray structure of the human APP-E2 domain

We identified a new tetragonal crystal form with improved diffraction properties that grew from cadmium-containing crystallization buffer. Using a partial molecular replacement (MR) solution with the *Caenorhabditis elegans* APL-1 E2 structure [Protein Data Bank (PDB) ID: 3K66[20]] as search model, we identified protein-bound cadmium atoms from anomalous difference Fourier maps. Final phases were calculated by single anomalous dispersion (SAD), resulting in a well-defined experimental electron density map. The structure was build and refined to 2.0 Å resolution, showing good *R*-factors and stereochemistry (Table 1). Exclusively composed of α-helical secondary structure, the molecule adopts an elongated shape spanning ~95 Å×35 Å× 25 Å (Fig. 1a). The short N-terminal helix α-A[14] was not observed in our tetragonal crystal form. The fold of the E2 domain is dominated by the central ~ 90-Å-long helix α-C, which is in contact to all other helices. Helix α-B (His313–Gln344) and the first 36 amino acids of the central helix α-C (Lys350–Arg385) contribute to a coiled-coil like fold. The C-terminal part of helix α-C (Val386–Gln406) together with helices α D (Arg411–Asp444), α-E (Lys446–Tyr474) and α-F (Val479–Gln492) constitutes a four-helix bundle enclosing a small hydrophobic core. The strict heptad repeat pattern is distorted in the E2 N-terminal coiled-coil like region as noted before.[14] Analysis of the contact surfaces of those helices revealed a similar solvation free-energy gain ($\Delta_i G$) for different E2 structures (Table 2). Hence, different relative orientations of these helices result in similar hydrophobic inter-helix contacts, explaining the high flexibility observed in previous structural studies of the human E2 domain.[14,16,21]

### Conserved intramolecular copper/zinc binding site in APP-E2

Interestingly, cadmium ions present in the crystallization buffer bound at various intermolecular (Cd3, Cd4, Cd5, Cd6 and Cd8) and intramolecular

**Table 1.** Data collection and refinement statistics

| | Data set | | | | | |
|---|---|---|---|---|---|---|
| | $Cd^{2+}$ lowE | $Cd^{2+}$ | $Zn^{2+}$ Peak | $Zn^{2+}$ lowE | $Cu^{2+}$ Peak | $Cu^{2+}$ lowE |
| *Data collection statistics* | | | | | | |
| Wavelength (Å) | 1.600 | 0.918 | 1.282 | 1.284 | 1.378 | 1.382 |
| Resolution limit (Å) | 2.7 | 2.0 | 2.4 | 2.5 | 2.6 | 2.7 |
| Unit cell parameters | | | $P4_3$ | | | |
| *a* (Å) | 39.3 | 39.7 | 39.7 | | 39.8 | |
| *c* (Å) | 125.9 | 126.2 | 125.8 | | 126.5 | |
| Completeness (%)[a] | 100.0 (100.0) | 100.0 (100.0) | 98.3 (89.0) | 99.7 (98.4) | 98.2 (88.3) | 99.8 (99.4) |
| $R_{merge}$ (%)[a] | 9.1 (42.2) | 5.6 (38.6) | 2.9 (7.9) | 3.4 (7.9) | 3.4 (9.9) | 3.6 (10.2) |
| $\langle I/\sigma_I \rangle$[a] | 46.2 (8.7) | 14.0 (3.4) | 27.1 (12.1) | 22.8 (13.2) | 23.5 (10.0) | 21.1 (10.1) |
| Redundancy[a] | 43.2 (33.8) | 4.2 (4.1) | 4.0 (3.2) | 4.1 (4.0) | 4.1 (3.5) | 4.0 (3.8) |
| *Refinement statistics* | | | | | | |
| Structure | $Cd^{2+}$ | | $Zn^{2+}$ | | $Cu^{2+}$ | |
| Resolution (Å) | 28.0–2.0 | | 28.0–2.4 | | 25.7–2.6 | |
| Unique reflections[b] | 12,503/647 | | 7020/433 | | 5597/341 | |
| $R_{work}$ (%)/$R_{free}$ (%) | 19.8/23.7 | | 20.4/24.5 | | 20.6/23.9 | |
| Nonhydrogen atoms | | | | | | |
| Protein | 1509 | | 1535 | | 1543 | |
| Water | 95 | | 79 | | 63 | |
| Metal ions | 9 | | 9 | | 9 | |
| Acetate ions | 8 | | 4 | | 4 | |
| *B*-factors (Å$^2$) | | | | | | |
| Overall/Wilson plot | 41.0/31.2 | | 36.7/40.2 | | 39.7/50.0 | |
| Protein | 40.6 | | 36.3 | | 39.6 | |
| Water | 47.5 | | 44.8 | | 43.0 | |
| Metal ions | 40.5 | | 40.7 | | 44.6 | |
| Acetate ions | 46.3 | | 32.9 | | 35.5 | |
| RMSDs | | | | | | |
| Bond lengths (Å) | 0.0073 | | 0.0049 | | 0.0048 | |
| Bonded *B*-factors (Å$^2$) | 3.6 | | 3.1 | | 2.6 | |

[a] Values given in parenthesis represent the highest-resolution shell. (Data collection: $Cd^{2+}$ lowE, 2.85–2.70 Å; $Cd^{2+}$, 2.11–2.00 Å; $Zn^{2+}$ peak, 2.53–2.40 Å; $Zn^{2+}$ lowE, 2.64–2.50 Å; $Cu^{2+}$ peak, 2.74–2.60 Å; $Cu^{2+}$ lowE, 2.85–2.70 Å; Refinement: $Cd^{2+}$, 2.09–2.00 Å; $Zn^{2+}$, 2.40–2.51 Å; $Cu^{2+}$, 2.60–2.72 Å.)
[b] Work/free.

sites (Cd1, Cd2, Cd7 and Cd9) (Fig. 1a). Most interestingly, the cadmium ion Cd1 at metal binding site M1 is surrounded by four histidine side chains (His313, His382, His432 and His436) (Fig. 1b; for stereo view, see Fig. S1a) of helices α-B, α-C and α-D in multiple coordination geometries. Similarly, helices α-C, α-D and α-E contribute to multiple binding states of Cd2 by Glu387, Asp429, His458 and a defined water molecule at metal binding site M2 (Fig. 1b; for stereo view, see Fig. S2a). Cd7 and Cd9 are bound by one amino acid side chain only, corresponding to weak binding sites that show a low occupancy in the structure. In consequence, both the E2 molecule and the crystal lattice are stabilized by a large number of defined cadmium ions, resulting in reduced flexibility of the molecule and high diffraction power of this crystal form.

The metal binding sites M1 and M2 provide coordination spheres suited for intramolecular binding of physiological transition metal ions such as copper and zinc. To probe the competitive displacement of $Cd^{2+}$, we soaked the crystals in a solution supplemented with either $Cu^{2+}$ or $Zn^{2+}$ in addition to $Cd^{2+}$. Two complete data sets were collected in the vicinity of the K absorption edge for each of the two elements (Table 1) in order to calculate element-specific anomalous double difference electron density maps[25] (Fig. 1c and d; for stereo view, see Fig. S1b and c and Fig. S2b and c).

$Zn^{2+}$ specifically replaces exceeding cadmium ions at binding site M1 and is coordinated by three histidines (His382, His432 and His436) as well as one water molecule in an almost tetrahedral geometry (Fig. 1c; for stereo view, see Fig. S1b). Upon specific replacement of $Cd^{2+}$ by $Cu^{2+}$, the electron density of His313 becomes well defined, and four histidines form a coordination sphere best described as tetrahedrally distorted square planar geometry (Fig. 1d; for stereo view, Fig. S1c). At metal binding site M2, the bound cadmium ion Cd2 was only partially replaced by $Zn^{2+}$ and not affected by $Cu^{2+}$ in the soaked crystals (Fig. 1c and d; for stereo view, see Fig. S2b and c). This observation indicates high specificity of M1 for $Zn^{2+}$ and $Cu^{2+}$ but low specificity of site M2 for these metal ions. The conservation analysis of both internal metal

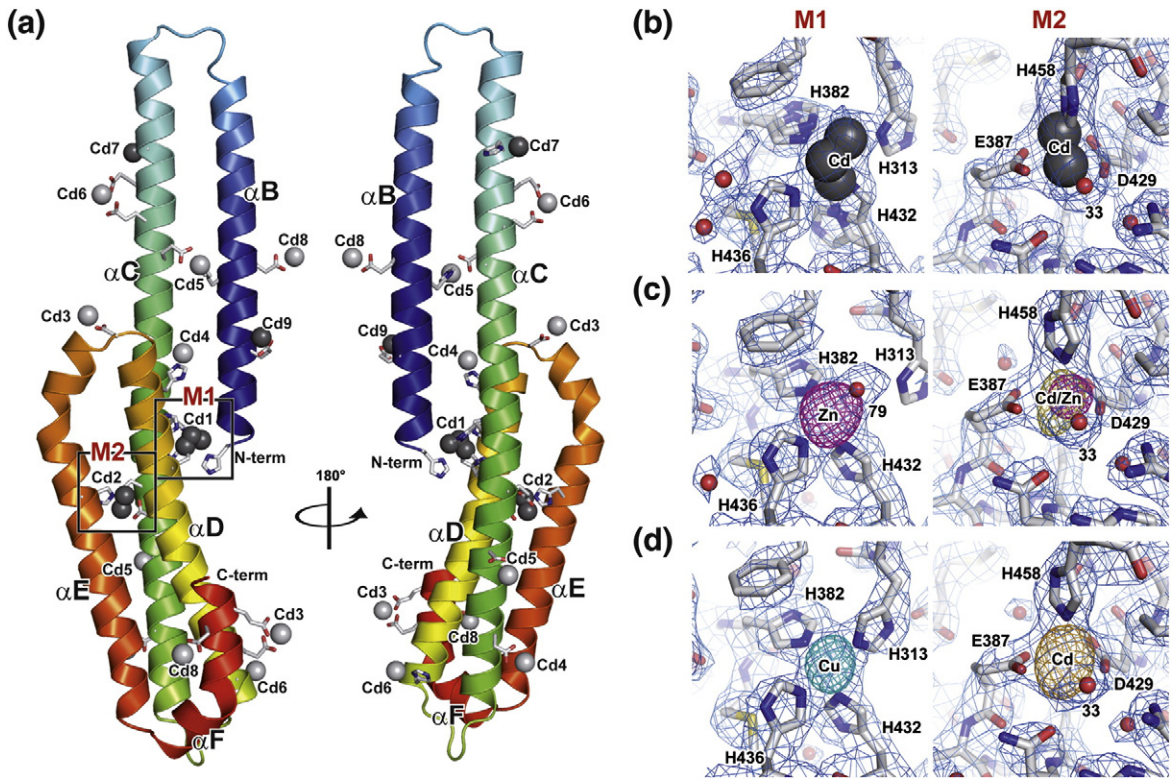


**Fig. 1.** Structure of the APP-E2 domain. (a) Cartoon representation of the APP-E2 domain with intramolecular (dark-gray spheres) and intermolecular (light-gray spheres) bound cadmium ions. The color gradient from blue to red indicates progression of the protein chain from the N- to the C-terminus. Amino acid side chains involved in metal coordination are shown as sticks. Crystallographic symmetry mates of cadmium ions were included in the picture to visualize the crystal contacts mediated by cadmium. The rectangles highlight the two intramolecular metal binding sites (M1 and M2), characterized by a complex coordination sphere. (b–d) Intramolecular metal binding sites M1 and M2. The electron density of the composite annealed $2F_o - F_c$ omit map contoured at 0.9 σ is shown in blue. (b) Cadmium occupied state: Both binding sites show multiple conformations of coordinating residues and cadmium ions. Cadmium ions are represented by spheres colored dark gray. (c) In $ZnCl_2$-soaked crystals, cadmium is replaced completely by zinc at site M1 and partially at site M2, indicated by the zinc-specific anomalous double difference density map contoured at 7 σ (magenta). (d) In $CuCl_2$-soaked crystals, cadmium is completely replaced by copper at site M1 but not at site M2, indicated by the copper-specific anomalous double difference density contoured at 7 σ (cyan). (b and c) The anomalous difference map at low energy, representing bound cadmium, is contoured at 5 σ (yellow).

binding sites is in excellent agreement with this observation. Alignments of APP, APLP1 and APLP2 sequences show that His313, His382, His432 and His436 at site M1 are highly conserved within the APP superfamily, including APLP1 and APLP2 (Fig. 2). In contrast, a similar conservation pattern of the amino acids at site M2 was not observed.

## Binding of copper/zinc in solution

The ability of the E2 domain to bind copper and zinc in solution was confirmed in an ultrafiltration-based retention assay (Fig. 3a). Both copper and zinc ions accumulated in the retenate of the ultrafiltration device upon APP-E2 concentration, but not in the

**Table 2.** Interaction within the N-terminal coiled-coil of different E2 structures

| Molecule/structure | Residues in helix α-B | Residues in helix α-C | Interaction interface (Å$^2$) | Free-energy of interaction $\Delta_i G$ (kcal/mol) |
|---|---|---|---|---|
| APP $Cu^{2+}$ bound[a] | 313–347 | 350–388 | 816 | −13.7 |
| APP metal free (PDB ID 1RW6)[b] | 369–403 | 406–444 | 771 | −18.5 |
| APL-1 metal free (PDB ID 3K66)[c] | 248–282 | 292–330 | 754 | −17.2 |

[a] Numbering according to APP isoform $APP_{695}$.
[b] Numbering according to APP isoform $APP_{751}$.
[c] *C. elegans* APL-1.

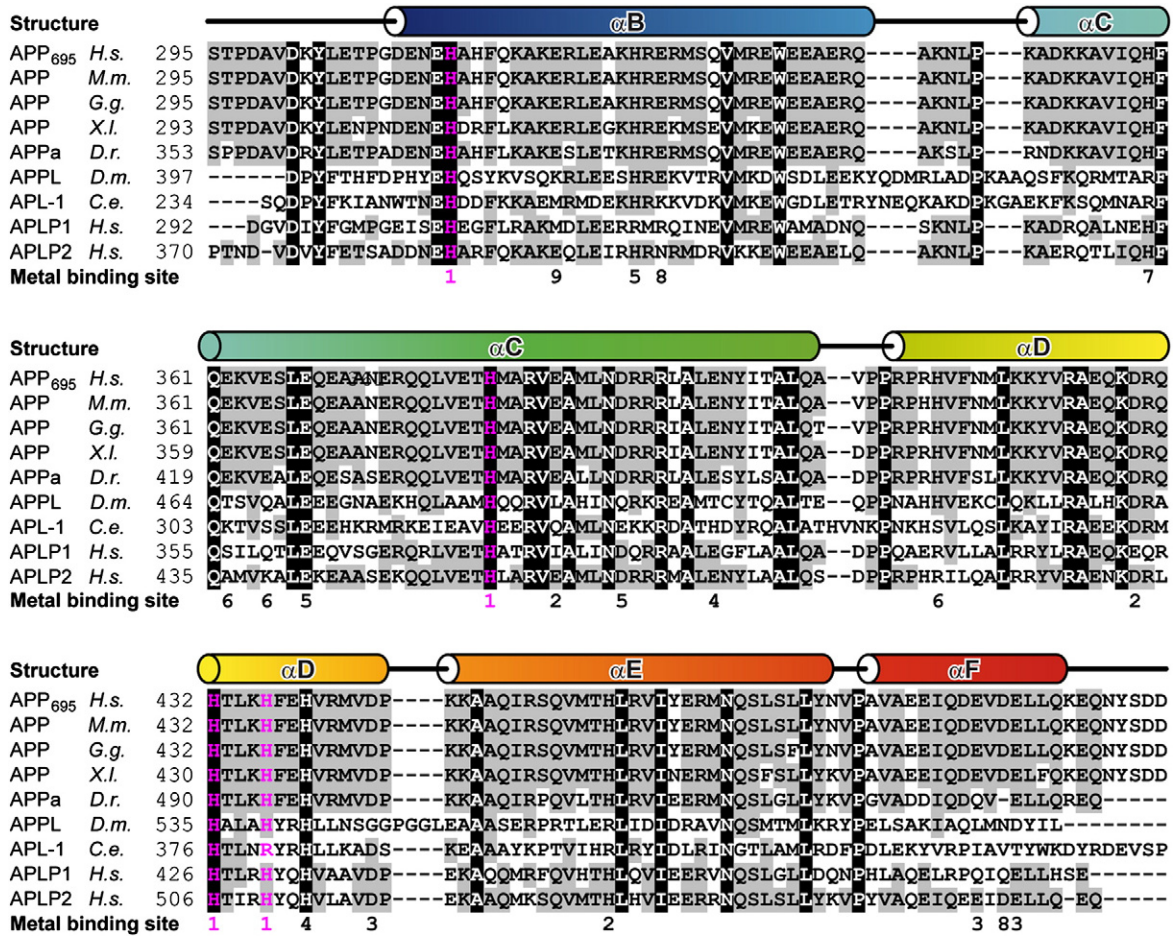


**Fig. 2.** Conservation analysis. Structure-based sequence alignments of vertebrate and invertebrate APP homologues and human APP-like proteins. Sequence similarities are highlighted in gray, and identical amino acids are shown in white on a black background. The ideogram on top of the alignment indicates α helical regions in the structure. The color gradient maps the sequence to the cartoon representation of the structure shown in Fig. 1a. Amino acids involved in the binding of cadmium ions are designated by numbers corresponding to the respective $Cd^{2+}$ binding site below the alignment. The highly conserved histidines involved in binding of copper and zinc at site M1 are highlighted in magenta.

controls. Several of the intermolecular metal binding sites can at least be partially occupied by copper or zinc ions (Fig. S3). To avoid these intermolecular contacts and hence precipitation of the E2 domain in solution, we always used 50 mM Tris as buffer to complex $Cu^{2+}$.

Determination of the binding strength by isothermal titration calorimetry (ITC) revealed tight binding of copper to the E2 domain (Fig. 3b), characterized by an apparent dissociation constant $K_{dapp}$ of 610 nM (Table 3), which has to be corrected, however, for the competition by the ligand Tris and its pH-dependent protonation.[26] The exact coordination chemistry of $Cu^{2+}$ by Tris is, unfortunately, not precisely known; for example, tertiary $Cu(Tris)_2$ and quinary $Cu(Tris)_4$ complexes are described in the literature. However, all models agree about the initial formation of a binary Tris–$Cu^{2+}$ complex, described by a formation constant $pK_{1(Tris)}$ of ~4. Considering only this first complexation step for correcting the apparent $K_{dapp}$, a binding constant $K_d$ of 13 nM was calculated as upper (weakest) limit. A similar calculation assuming the quinary $Cu(Tris)_4$ complex[26] results in values as low as 2 pM. In addition, we determined the apparent $K_{dapp}$ as function of the Tris concentration showing a linear dependency (Fig. 3c). This was initially surprising, as we expected a higher-order relationship due to the stoichiometry of described $(Tris)_n$–$Cu^{2+}$ complexes. Based on the linear dependency, we concluded that the higher-order association steps [i.e., $Cu(Tris)_n \rightarrow Cu(Tris)_{n+1}$] are of less influence on the effective copper concentration under the used conditions and that our correction with $pK_{1(Tris)}$ is quite adequate. The used concentrations of Tris were chosen such that it was always in large excess (>100-

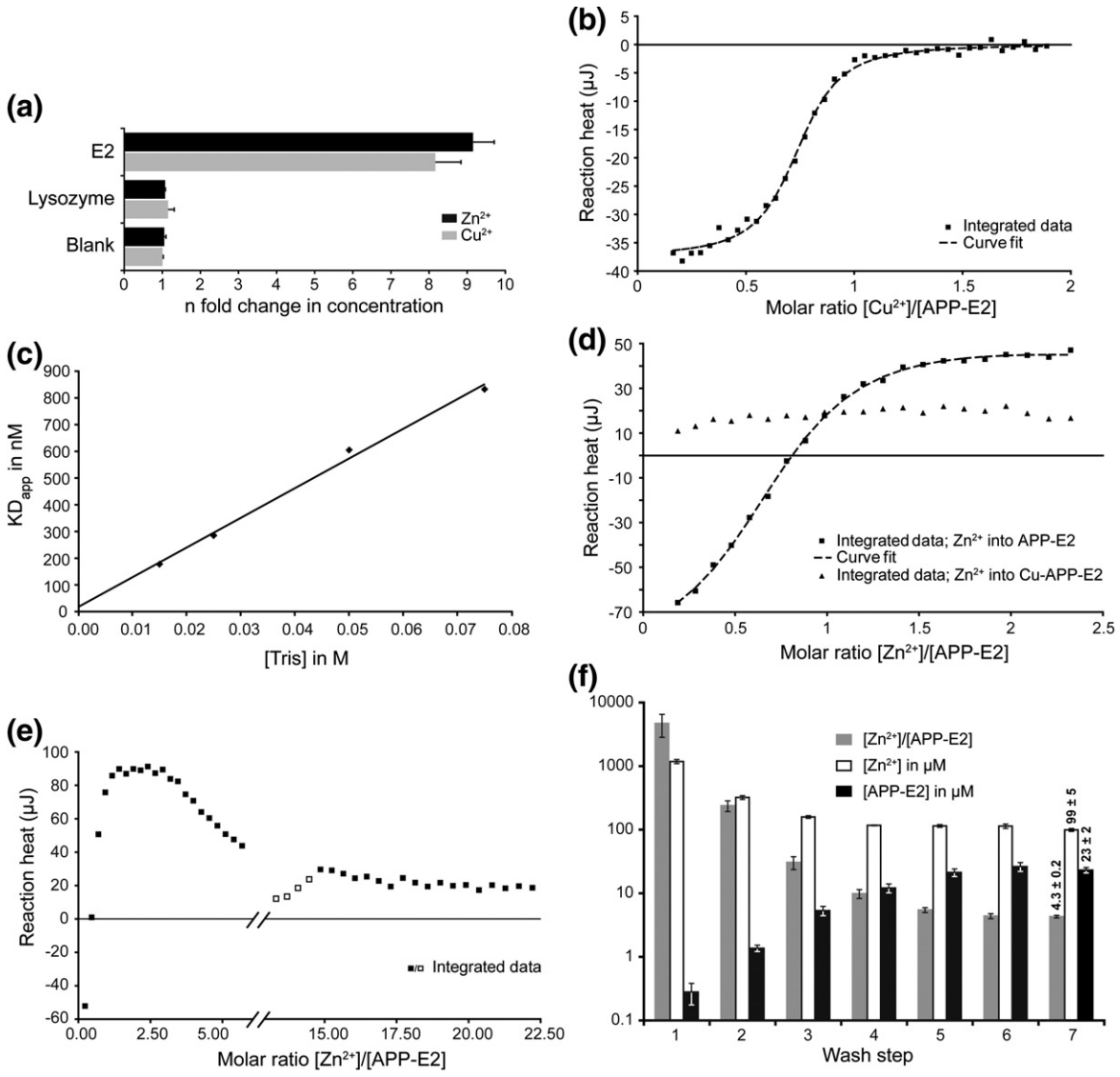


**Fig. 3.** Binding of zinc and copper to APP-E2 in solution. (a) Metal retention assay probing the capability of the protein to retain metal ions upon concentration. The ratio of the metal concentration in the retenate relative to the initial metal concentration is shown after 8-fold concentration by centrifugation in the presence of the E2 domain and of a control protein (lysozyme) and in the absence of any protein (blank). (b) ITC binding curve of copper to APP-E2. (c) Dependence of $K_{dapp}$ on Tris concentration. $K_{dapp}$ of copper to APP-E2 was measured at 15 mM, 25 mM, 50 mM and 75 mM Tris in ITC experiments. $K_{dapp}$ was plotted as a function of [Tris], linearly fitted and evaluated assuming competition of APP-E2 with Cu(Tris) according to $K_{dapp} = K_d + K_{1Tris} \times K_d \times [\text{Tris}]$. (d) ITC binding curve of zinc to APP-E2. Filled triangles represent integrals for a zinc titration experiment with copper-pre-saturated APP-E2. The exothermic binding reaction observed for binding of zinc to APP-E2 is completely suppressed if copper is bound to the protein. (e) ITC measurements at high Zn/protein ratios. The ITC peak integrals of the first and third titration runs of a serial titration experiment to achieve zinc saturation are shown as squares. Filled squares represent reliable data points, whereas open squares mark data points adversely affected by dilution due to the refilling procedure necessary after each titration run. (f) Experimental determination of the average number of zinc ions bound to APP-E2. Initial precipitation by excess zinc followed by several wash steps resulted in a stable equilibrium ratio of zinc-bound protein in the liquid phase and in the solid phase. Concentrations of zinc and protein and the ratio between zinc and protein are shown for seven subsequent wash steps, when the equilibrium was reached. The final ratio is 4.3 total (corresponding to one tight and 3.3 weak) zinc binding sites per E2 molecule.

fold) over $Cu^{2+}$ in order to suppress the occupation of weaker $Cu^{2+}$ binding sites. In all ITC experiments, the binding isotherms showed a single inflection point and were indicative of one set of identical binding sites with stoichiometries of ~1 (Fig. 3b and data not shown). Correspondingly, a linear extrapolation results in a $K_d$ of ~20 nM as intersection point with the ordinate in good

**Table 3.** Binding constants of $Cu^{2+}$ and $Zn^{2+}$ to APP-E2 determined by ITC

| | Cu–APP-E2 | | |
|---|---|---|---|
| | $K_{dapp}$ | $K_d$ | Zn–APP-E2 |
| $K_{d1}$ (μM) | 0.61 ± 0.23 | 0.013 ± 0.005 | 3.9 ± 1.5 |
| $K_{d2}$ (mM) | — | | 2.6 ± 1.2[a] |
| $\Delta H_1$ (kJ/mol) | −19.9 ± 0.9 | | −16.6 ± 0.6 |
| $\Delta H_2$ (kJ/mol) | — | | 1200 ± 600 |
| $n_1$ | 0.70 ± 0.03 | | 0.7 ± 0.2 |
| $n_2$ | — | | 3.3[b] |

[a] Not statistically significant in curve fit as confidence intervals exceed the measured values at a confidence level of 99%.
[b] Determined independently and fixed during curve fit.

agreement with our correction model applying $pK_{1(Tris)}$ (see also Materials and Methods).

To study the formation of the $Zn^{2+}$–APP-E2 complex in ITC experiments, the addition of specific zinc chelators to the Hepes buffer resulted in apparent binding constants that were too low for numeric evaluation. Therefore, we measured zinc binding in the absence of a zinc-specific chelator and evaluated the ITC data as arising from multiple zinc binding sites including unspecific association of zinc ions to the protein surface. The binding isotherm showed an initial exothermic reaction corresponding to one strong interaction followed by an endothermic contribution apparently arising from multiple weak binding sites (Fig. 3d). ITC experiments at high zinc-to-protein ratios (Fig. 3e) showed a continuous, smooth decline of the endothermic reaction. No saturation of zinc binding could be observed, and the protein begun to precipitate at zinc-to-protein ratios exceeding 5:1. Hence, the total number of zinc binding sites at APP-E2 was determined experimentally (Fig. 3f) and used to evaluate the binding curves employing a model of two sets of independent binding sites. The resulting dissociation constants $K_{d1}$ of 3.9 μM and $K_{d2}$ of 2.6 mM have to be regarded as upper (weakest) limit since $K_{d2}$ is determined not statistically significant in the fit (Table 3). A possibly lower $K_{d2}$ necessarily results in a decreased $K_{d1}$ value. Higher values of $K_{d2}$ however would affect $K_{d1}$ slightly but would

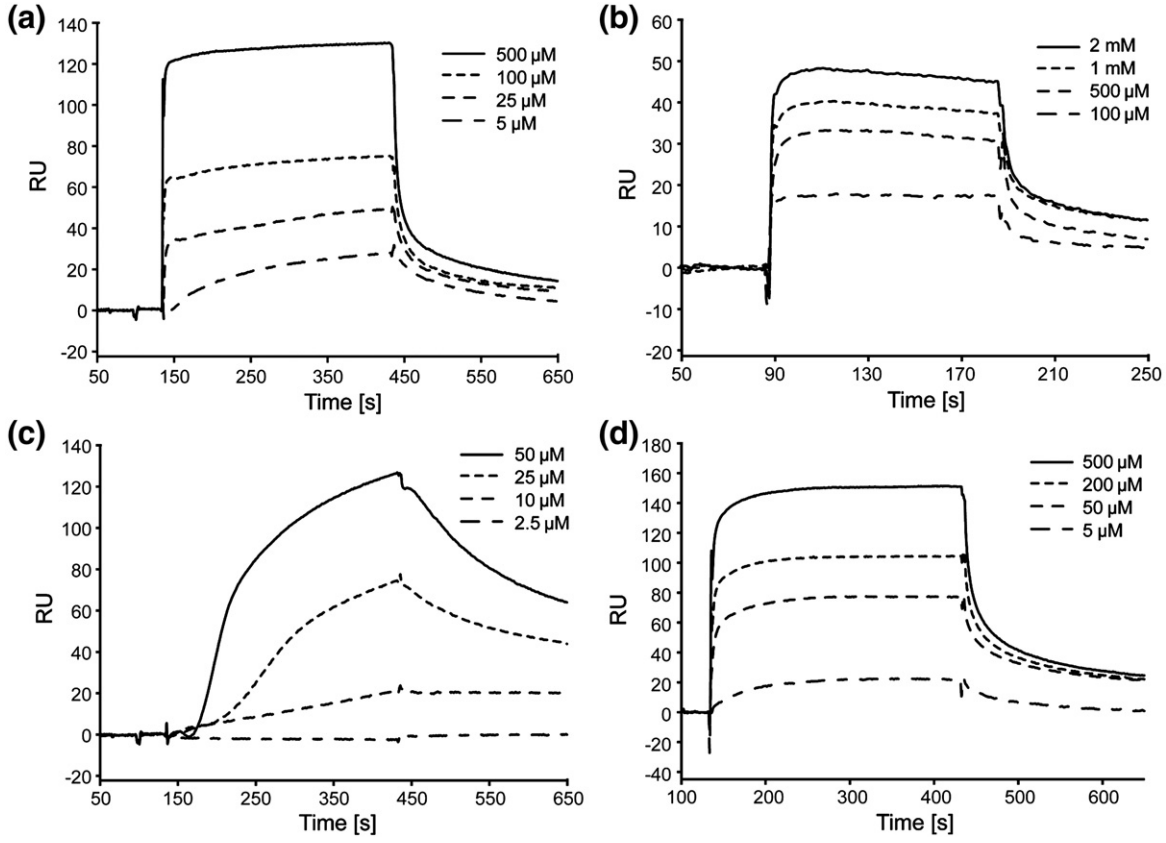


**Fig. 4.** Metal ions induce conformational changes in APP-E2. (a and b) Overlays of representative SPR sensorgrams obtained from injections of zinc chloride and (c and d) copper chloride solutions. For suppression of weak metal–protein interactions, spectra were recorded in the presence of (b) 20 mM citrate or (d) 20 mM Tris. Ions at indicated concentrations were injected at a flow rate of 30 μl/min for (a, c and d) 300 s or (b) 100 s, respectively, followed by dissociation of the metal–protein complex in running buffer.

cause an increase in $\Delta H_2$ to values even higher than 1200 kJ/mol, unlikely for non-covalent interactions.

To verify that zinc and copper compete for the same binding site in solution, we repeated the zinc binding experiments with APP-E2 preparations pre-saturated with copper. If copper ions are bound to the protein, the exothermic reaction upon $Zn^{2+}$ addition is completely missing from the ITC profile, as expected for a competitive metal binding site (Fig. 3d). In contrast, the unspecific binding is still observed as indicated by the continuous endothermic signal.

## Metal binding causes large conformational changes in APP-E2 in solution

Next, we evaluated binding of $Cu^{2+}$ and $Zn^{2+}$ to APP-E2 by surface plasmon resonance (SPR) analysis. Interestingly, the addition of $Zn^{2+}$ (Fig. 4a and b) and $Cu^{2+}$ (Fig. 4c and d) to APP-E2 covalently attached to the chip surface resulted in a large increase in the SPR signal up to ~130 response units (RU). The rise in RU upon injection of metal ion solutions is too high to be explained by binding of single metal ions. Furthermore, the binding curves exhibit complex functions that cannot be attributed to a standard model of binding kinetics. This indicates structural rearrangements of the protein bound to the sensor chip surface. To analyze the contribution of weaker metal ion binding sites to the binding curves, we added specific chelators of $Zn^{2+}$ (Citrat) and $Cu^{2+}$ (Tris), which reduced the complexity of the binding curves (Fig. 4b and d). This indicates that the SPR signal increase can be partially explained by multiple binding sites on the protein and that the chelators compete with the weaker metal binding sites. However, the unexpectedly high SPR signal increase of ~50 RU ($Zn^{2+}$) and ~150 RU ($Cu^{2+}$) still suggests major conformational rearrangements in the presence of the chelators.

## Conformational differences between metal-bound and metal-free structures of the E2 domain

A structural alignment of the C-terminal parts (Ala388–Gln492) of the copper-bound (this work) and the metal-free (PDB ID: 1RW6[14]) human APP-E2 structures revealed a specific reorientation of the N-terminal segment (Fig. 5a). In the metal-free protein, helix α-B and the N-terminal part of helix α-C are highly flexible and can adopt multiple conformations. Conformational dynamics of this segment were confirmed in APL-1[20] and APLP1,[16] underscoring a general mode of flexibility of the E2 domains in the APP superfamily. The functional consequences of APP-E2's flexible nature were unknown until now, but they are apparent in the context of metal binding. Binding of ions such as $Cu^{2+}$ requires a specific coordination geometry and hence a specific conformation of the APP-E2 domain. The N-terminal coiled-coil, consisting of the N-terminal half of helix α-C and the preceding helix α-B, is rotated as rigid body by 12° (angle of α-carbon segments between Ala355 and Ala388) (Fig. 5b). Rotation occurs at a hinge region between His382 and Ala388. An additional movement twists helices α-B and α-C around each other by about 7° in the metal-bound form (Fig. 5c). In consequence, His313 at the N-terminus of helix α-B relocates more than 8 Å toward the metal binding center (Fig. 5d).

Coordination of copper requires the proper orientation of the four coordinating histidine side

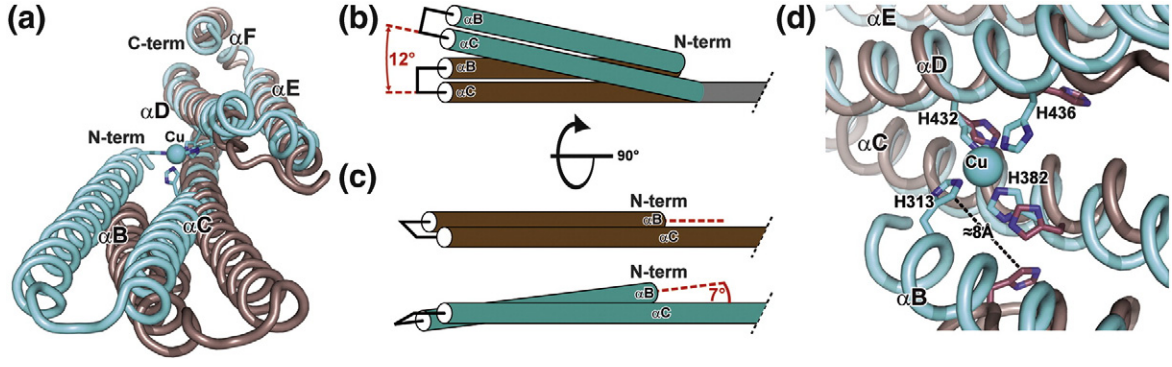


**Fig. 5.** Conformational differences between metal-bound and metal-free APP-E2 structures. (a) Superposition of the C-terminal parts of metal-bound APP-E2 (Arg385–Leu490, $APP_{695}$ numbering) and metal-free APP-E2 (Arg441–Leu546, $APP_{751}$ numbering)[14] in cyan and brown, respectively. To mark the metal binding center in the structure, the histidine side chains of the copper coordination sphere are shown as sticks, and the central copper ion is represented as a cyan sphere. (b) A hinge region in helix α-C causes a concerted, rigid-body rotation of helix α-B and the N-terminal half of helix α-C by 12° in the metal-bound APP-E2 domain. (c) Fixation of helix α-B in the copper-bound state of the APP-E2 domain requires a twist of 7° in the N-terminal coiled-coil. (d) Detailed view of the copper and zinc binding site M1 of the APP-E2 domain and the structural rearrangements following metal binding. The color scheme is as in (a).

chains (His313, His382, His432 and His436). In contrast, no specific orientation of the N-terminal helix should be required in the zinc-bound state as a water molecule replaces His313 as ligand. Consequently, the available structural data imply at least three different conformational states of the APP-E2 domain, differing in the flexibility of the N-terminal coiled-coil: In the metal-free protein, helix α-B and the N-terminal part of helix α-C are highly flexible. If zinc is bound, the central helix α-C is stabilized as His382 participates in metal coordination, but movement of the amino acids located N-terminal of His382 is still possible. However, binding of copper requires concerted structural rearrangements to establish the required coordination sphere, and hence, movement of the coiled-coil helices is restricted.

### Binding of copper/zinc stabilizes metal-dependent conformations of the APP-E2 domain in solution

In the crystals, we probably "trapped" one conformation of the E2 domain. For this reason, movement of the N-terminal helix is restricted by the crystal packing, even if the binding site M1 becomes occupied by $Zn^{2+}$. In order to verify the expected metal-specific conformational states in solution, we performed limited proteolysis and circular dichroism (CD) spectroscopy experiments.

Previously, a stable fragment was identified in limited proteolysis experiments with trypsin, comprising the amino acids Val385–Arg501 of $APP_{695}$[21] next to the recently mapped cleavage site of meprin β.[27] Interestingly, the N-terminal boundary exactly matches the hinge region identified in the E2 domain (see above). The stable fragment hence lacks a major part of the central helix α-C and helix α-B, including the metal-coordinating residues His382 and His313. As binding of $Cu^{2+}$ and $Zn^{2+}$ is expected to specifically affect the flexibility of helices α-C and α-B and consequently the susceptibility to trypsin cleavage, we performed limited proteolysis of the E2 domain in the presence of these ions (Fig. 6a). The N-termini of the resulting peptide fragments were determined by Edman sequencing (Table 4). The major trypsin cleavage products in the absence of any metal ions indeed indicated rapid degradation of helices α-C and α-B N-terminal of Lys354 (fragment 2), Arg375 (fragment 3) and Arg385 (fragment 4). In contrast, the remaining C-terminal fragment 4 starting at Val386 remains stable for more than 1 h in the presence of trypsin once the N-terminal coiled-coil region is cleaved off. This observation is in agreement with the elevated *B*-factors and hence flexibility of the amino acids N-terminal of Ala355 (Fig. 6b).

Addition of copper to the proteolysis reaction stabilizes especially fragment 1, corresponding to the full-length protein, and to a lesser extent also

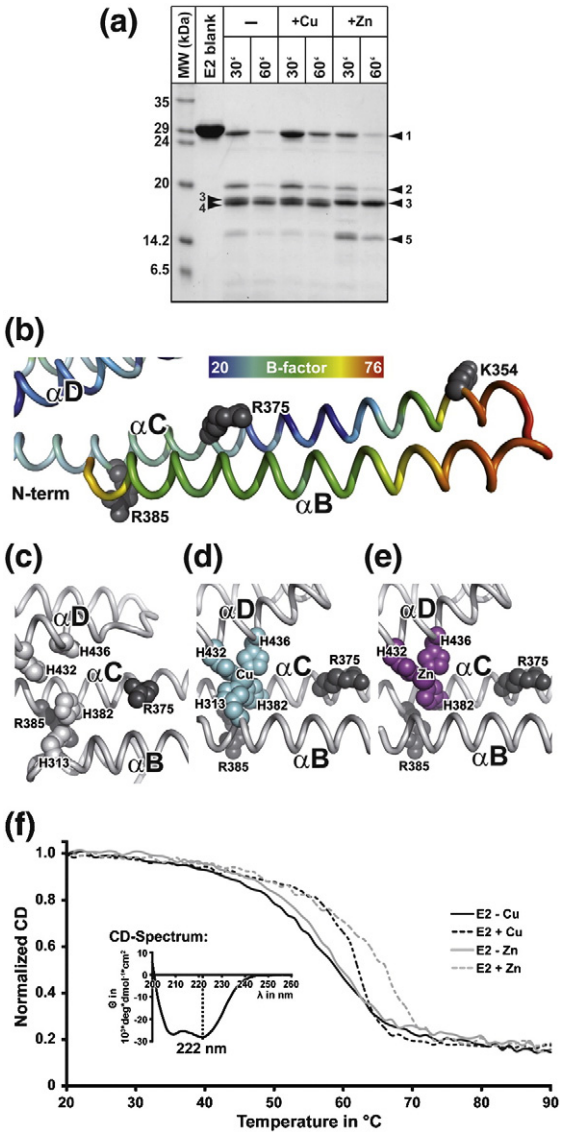


**Fig. 6.** Stabilization of metal-specific conformations of the E2 domain in solution. (a) Limited proteolysis experiments with trypsin. Protease cleavage products are marked by arrowheads, and cleavage sites are listed in Table 4. Note the double band 3/4 as also evidenced by our sequencing data. Addition of copper to the protein increases the stability of the N-terminal segment (fragment 1), whereas zinc ions abrogate cleavage at Arg385 and result in the accumulation of fragment 3. (b) The N-terminus of the E2 domain is shown in detail according to the *B*-factors of the cadmium-bound structure. The side chains shown in sphere representation (dark gray) mark the trypsin cleavage sites in the structure. (c–e) Close-up of the region encompassing metal binding site M1 (c) in the metal-free form[14], (d) in the copper- and (e) in the zinc-bound states. (f) A typical α-helical CD spectrum of the APP-E2 domain with a characteristic minimum at 222 nm (insert). Addition of metals (broken lines) to APP-E2 (respective controls represented by continuous lines) results in tighter folding of APP-E2 at high temperatures, indicated by CD melting curves.

**Table 4.** Fragments generated by limited trypsin digestion

| Fragment[a] | N-terminal sequence | Cleavage site | Influence on cleavage site |
|---|---|---|---|
| 1[b] | STPD[c] | | |
| 2 | AVIQ | (K354)↓A355[d] | $Cu^{2+}$ |
| 3 | QQLV | (R375)↓Q376[d] | $Cu^{2+}$ |
| 4 | VEAM | (R385)↓V386[d] | $Zn^{2+}$; $Cu^{2+}$ |
| 5 | STPD[c] | | |

[a] Numbers according to Fig. 6.
[b] Full-length protein after removal of a few C-terminal linker residues that were left behind after V8 cleavage but do not belong to the native APP sequence.
[c] The sequence STPD corresponds to the very N-terminus of the construct.
[d] In parentheses: S1 residue, C-terminally cleaved by trypsin.

fragments 2 and 3 (Fig. 6a). This observation is in excellent agreement with the structural properties of the copper-bound E2 domain: Coordination of copper requires a specific orientation of His313, His382, His432 and His436 and hence a proper orientation of helices α-B, α-C and α-D. *Vice versa*, helices α-B, α-C and α-D are cross connected, and their movement is necessarily restricted upon copper binding, reducing the overall flexibility and preventing the protein from proteolytic attack (Fig. 6c and d). Once the N-terminal helix is cleaved off by the protease, only three histidine side chains are left for copper coordination, which is expected to weaken the binding significantly. Accordingly, the stabilizing effect of copper is expected to be weaker for the smaller fragments 2 and 3 compared to fragment 1 as seen in Fig. 6a.

Due to the different coordination sphere seen for APP-E2-bound $Zn^{2+}$, not involving His313 of helix α-B, we expected a different effect of this ion on APP-E2 stability. Indeed, if $Zn^{2+}$ was present in the cleavage reactions, a very strong site-specific protection was observed. Trypsin cleavage at Arg385 completely disappeared, and fragment 3 accumulated (Fig. 6a). The abundance of the N-terminal fragment 5 also increased. Apparently, zinc specifically stabilizes the region between Arg375 and Arg385 including the coordinating His382. It does, however, still allow flexibility in the region N-terminal of Arg375 as His313 at the N-terminus of helix α-B does not contribute to $Zn^{2+}$ binding (Fig. 6e).

In agreement with the limited proteolysis data, we observed a metal-dependent melting behavior of the APP-E2 domain by CD spectroscopy (Fig. 6f). Addition of copper and zinc results in an increased CD signal at 222 nm and hence increased α-helical content of the protein at high temperatures. The zinc-bound E2 domain unfolds continuously in between 50 °C and 70 °C, and the melting temperature increased from 57.8 ± 0.3 °C to 64.2 ± 0.3 °C upon addition of 10 μM $Zn^{2+}$. Copper binding to the E2 domain is accompanied by a largely altered unfolding behavior of the protein. In addition to the elevated melting temperature (57.3 ± 0.3 °C in plain buffer *versus* 61.0 ± 0.0 °C after addition of 10 μM $Cu^{2+}$), an increased unfolding cooperativity is observed in the presence of copper. The protein collapses at temperatures above 61 °C, indicated by an increased slope of the melting curve. Our structural data give a good explanation for this cooperative collapse: The N-terminal coiled-coil is characterized by increased flexibility and is consequently expected to be more sensitive to heat-induced unfolding than the C-terminal helix bundle. Copper binding stabilizes the protein in general, but destabilization or even partial unfolding of the N-terminus at elevated temperatures will weaken the coordination of $Cu^{2+}$ by His313. Once this bond breaks, the affinity to copper decreases drastically, resulting in higher flexibility and rapid unfolding of helix α-B, which in turn triggers unfolding of the entire E2 domain. In contrast, zinc binding causes a local stabilization of helix α-C and the C-terminal core structure. It still allows flexibility of the N-terminal coiled-coil region and does not result in increased cooperativity during unfolding.

## Discussion

We have identified a novel crystallization condition of the APP-E2 domain and refined its structure to a resolution of 2.0 Å. Compared to previous attempts to crystallize the highly flexible E2 domain, the co-crystallization of the protein with metal ions resulted in strikingly improved diffraction quality of the crystals and lower overall *B*-factors. The structure of the E2 domain revealed an intramolecular metal binding site with high specificity and affinity for zinc and copper.

Four highly conserved histidine side chains at metal binding site M1 selectively provide a coordination geometry that fits to the first-row transition metals copper and zinc. In contrast, the larger cadmium ion is unspecifically bound in multiple states. Coordination of zinc is facilitated by three histidine residues and a water molecule, replacing the side chain of His313 as fourth ligand. The pH-dependent zinc binding properties of full-length APP[23] are in excellent agreement with a histidine-mediated coordination. Four histidine side chains of the E2 domain contribute to copper coordination at this site, including His313. This observation is in excellent agreement with the general coordination properties of copper ions in biological macromolecules, preferring nitrogen to oxygen ligands.[28]

The functional importance of the metal binding site of the APP-E2 domain is evident from the large conformational changes in the protein confirmed by SPR, the increased thermostability and the altered protease accessibility upon binding of copper and

zinc. The metal-free but not the metal-bound state of the E2 domain allows bending of the central elongated helix and reorientation of the N-terminal coiled-coil region. A comparable effect of metal binding was, for example, described for human endostatin,[29] requiring coordination of zinc by the otherwise flexible N-terminal region for its biological activity. Binding of copper and zinc to APP-E2 does not only prevent structural flexibility but also stabilize distinct conformations that depend on the exact coordination sphere. Copper binding by the E2 domain requires cooperative action of four sequentially distant histidine side chains stabilizing the overall structure. In contrast, the zinc-bound state affects particularly the central helix and the C-terminal helix bundle. These characteristics resemble a metal-ion-triggered conformational switch that converts the protein into different functional states, in principle similar to metal-dependent regulatory proteins such as calmodulin.[30] In contrast to the binary on/off switch of calmodulin, the competitive metal binding properties of the E2 domain implicate regulation in an even more complex manner, employing multiple functional states.

The central question arising is: Is the described competitive binding of $Zn^{2+}$ and $Cu^{2+}$ as well as the resulting conformational changes of physiological relevance? Membrane-bound and soluble APP are transported to and localized at synaptic terminals (e.g., Refs. 31–33). Maximum concentrations of more than 10 μM zinc[34] and/or copper[4] are reached during neuronal activity in hippocampal glutamatergic synapses, whereas basal levels of ~20 nM free zinc and ~50 nM free copper were measured in the brain interstitium[35] and in the cerebrospinal fluid,[36] respectively. We estimated a dissociation constant of the E2–zinc complex of lower than 4 μM, in the same order of magnitude as previously reported for full-length APP (0.75 μM),[23] indicating a significant affinity for zinc within its physiological environment. Interestingly, $Cu^{2+}$ binds tighter to APP-E2, again in excellent agreement with the biochemical properties of full-length APP (10 nM).[22] Already an underestimated correction for the competition with the buffer compound results in an absolute $K_d$ of lower than 13 nM. Correspondingly, copper displaces zinc from the protein, a competition also verified in respective ITC experiments. In consequence, the E2 domain of APP sensitively responds to elevated copper levels even in the presence of zinc. Sequence alignments reveal a high degree of conservation of this metal binding site among APP family proteins, including APLP1 and APLP2. This indicates its essential function also in APP-like proteins, which most likely follow a similar antagonistic copper- and zinc-dependent regulation scheme reflecting the functional redundancy described for the APP family members.[37] Consequently, misregulation of the E2 domain based on imbalanced levels of copper and zinc is expected to impair the proper function of APP and APP-like proteins. Interestingly, the metal binding site of the E2 domain offers an explanation for a number of previously unrelated findings in molecular detail.

A ferroxidase-like activity of the E2 domain is inhibited by zinc at micromolar concentrations but not by copper.[38] Based on our results, one might expect the activation of the oxidase activity of the E2 domain by copper at low concentrations of inhibitory zinc ions. This potential mechanism provides an elegant explanation of how APP could be activated to facilitate export of redox-active metal ions. Indeed, several studies showed that the neuroprotective α-secretase cleavage product sAPPα is involved in oxidative stress response.[39–41]

The protein ligands F-Spondin[42,43] and SorLA[44] can bind to the E2 domain and regulate the neuronal trafficking of APP. Strikingly, the interaction of E2 with these binding partners is inhibited in the presence of the strong metal chelator ethylene glycole tetraacetic acid.[42,44] The localization of APP is crucial for processing by regulated intramembrane proteolysis and hence for the production of Aβ.[3] Addition of copper to cells also affects the trafficking of APP to the cell surface[45] and reduces amyloidogenic processing.[46] Here we propose a mechanism connecting ligand- and metal-dependent regulation of APP: Metal binding specifically switches the conformation of the E2 domain, which in turn should modulate the interaction with its ligands and finally the trafficking of APP. This regulation scheme is also applicable to the E2 domains of APLP1 and APLP2. Both proteins contain the metal binding residues and are capable of interacting with F-Spondin.[42] Dysregulation of the neuronal metal homeostasis in AD should therefore interfere with the regulation of all APP family proteins. Malfunction of APP, APLP1 and APLP2 may therefore directly contribute to the pathology in AD.

Our excellent diffracting crystals enable a structure-guided approach to develop small molecules specifically influencing the metal-dependent conformations of the E2 domain. Such compounds are useful to investigate the conformation-dependent regulation of the E2 domain. Furthermore, they might prove useful to influence the cellular fate and function of APP and to modulate the pathological events leading to AD in future studies.

## Materials and Methods

### Expression and purification

APP-E2 comprising Ser295–Asp500 (numbering according to $APP_{695}$) was recombinantly expressed in *Escherichia coli* BL21(*DE3*)pRIL and purified by immobilized metal

ion chromatography as well as by gel permeation chromatography as described previously.[19] For crystallographic and biochemical studies, the C-terminal hexa-histidine tag was cleaved with either 20 U/mg protein coagulation factor Xa (Novagen) for 24 h at 20 °C or 1.5 μg/mg protein–V8 protease (Calbiochem) for 1 h at 25 °C, respectively. Protease and uncleaved protein were removed by application to either a Benzamidine Sepharose 4 FF column (GE Healthcare) combined with a HisTrap FF Crude column (GE Healthcare) in the case of factor Xa or a HisTrap FF Crude column combined with a HiTrap Heparin HP column (GE Healthcare) in the case of V8 protease.

### Crystallization and structure determination

Diffraction-quality crystals were grown by the sitting-drop vapor diffusion method at 20 °C, mixing equal volumes of 10 mg/ml protein solution and reservoir containing 0.1 mM Hepes (pH 6.4), 1 M sodium acetate, 10 mM $MgCl_2$ and 50 mM $CdSO_4$; 12.5% *R*(−)-2-methyl-2,4-pentanediol was added for cryoprotection. In competitive metal binding experiments, crystals were soaked in reservoir solution complemented with 10 mM $CuCl_2$ or $ZnCl_2$ in addition to 40 mM $CdSO_4$ for 12 h, including the cryoprotectant. For analysis of $Cu^{2+}$ and $Zn^{2+}$ binding, X-ray fluorescence scans were performed, and complete anomalous data sets were collected at either end of the respective K-absorption edges. Data sets were collected at 100 K at the synchrotron (BESSY II/BL14.1 and BL14.2/Berlin) and processed with programs of the CCP4 suite[47] (Table 1). A high-resolution data set extending up to 2.0 Å and a highly redundant SAD data set extending to 2.7 Å at low energy were measured using cadmium-containing crystals. Initial attempts to solve the phase problem by MR using the available structure of human APP-E2 (PDB ID: 1RW6[14]) failed, implicating major conformational differences. Finally, the phase problem was solved by a combination of MR and SAD. The PDB structure 3K66 (APL 1[20]) was modified with CHAINSAW,[48] and MR was calculated in Phaser.[49] Applying these phases to the cadmium SAD low-energy data set, we identified seven cadmium sites in the respective anomalous difference Fourier map, followed by SAD phasing and density modification in SHARP.[50] The initial model, build in Buccaneer,[51] was transferred to the 2.0 Å-resolved cadmium data set as well as to the copper and zinc peak data sets, manually revised in MAIN[52] and refined in CNS v1.3[53] (for details, see Table 1). The occupancies of the metal ions were refined by individual occupancy refinement in CNS v1.3.[53] All main-chain angles fall into the most favored and additionally allowed regions of the Ramachandran plot.[54] Bond length, dihedral angles and bond angles of His313, His382, His432 and His436 to $Cd^{2+}$, $Zn^{2+}$ and $Cu^{2+}$ were restrained to corresponding average values derived from the Cambridge Structural Database.[55] Composite annealed omit maps were calculated in CNS v1.3 omitting 2.5% of the final model. Element-specific "difference DANO maps" were calculated according to Ref. 25. PyMOL (DeLano Scientific LLC, USA†) was used for molecular graphics and the sequence-based structure alignments.

† www.pymol.org

### Contact analysis of the N-terminal coiled-coil

The interaction interface per protomer and the solvation free-energy gain upon interface formation corresponding to the hydrophobic interactions $\Delta_i G$ were calculated with PISA[56] (Table 2). The following structures were used for comparison: copper-bound APP-E2 (this work), metal-free APP-E2 (PDB ID: 1RW6[14]) and metal-free APL-1-E2 (PDB ID: 3K66[20]).

### Sequence alignment and analysis of APP-E2 conservation

Sequences of APP, APLP1 and APLP2 were aligned using MUSCLE[57] and manually edited to match the structural superposition of human copper-bound APP-E2 and *C. elegans* APL-1. The following sequences were obtained from the UniProt (UP) database[58] or GENEBANK to calculate the sequence alignments: *Homo sapiens* APP (UP code: D3DSD1), *Mus musculus* APP (UP code: Q6GR78), *Gallus gallus* APP (UP code: Q9DGJ8), *Xenopus laevis* APP (UP code: Q98SG0), *Danio rerio* APPa (UP code: Q90W28), *Drosophila melanogaster* APPL (UP code: P14599), *C. elegans* APL-1 (GENEBANK code: AAC46470.1), *H. sapiens* APLP1 (UP code: P51693) and *H. sapiens* APLP2 (UP code: Q06481).

### Metal retention assay

APP-E2 (50 μM; without His-tag) and 75 μM $CuCl_2$ in 50 mM Tris/HCl (pH 7.3), 150 mM NaCl or 75 μM $ZnCl_2$ in 20 mM Hepes/NaOH (pH 7.3) and 150 mM NaCl were concentrated 8-fold by ultrafiltration at 20 °C (Vivaspin 500, 5000 kDa molecular weight cutoff PES membranes; Sartorius Stedim Biotech). Samples without protein, or containing 50 μM lysozyme instead of APP-E2, served as controls. Metal ions in the retenate were quantified spectrophotometrically.[59] Each experiment was performed in triplicate, and the average ratio of the final concentration relative to the starting concentration ($c_{metal}/c_{metal,0}$) is given.

### Isothermal titration calorimetry

ITC was performed at the same conditions as the metal retention assays in a NANO ITC calorimeter (TA Instruments, USA) adding 0.4 mM $CuCl_2$ in 6-μl injections or 0.4 mM $ZnCl_2$ in 11-μl injections to the cell containing 40 μM protein. Blank enthalphies for titrations of metals in buffer were subtracted from peak integrals. Binding constants were calculated with the NanoAnalyze program (TA Instruments) using a model for a single set of identical binding sites ($Cu^{2+}$) and two sets of independent binding sites ($Zn^{2+}$). All titrations were performed in triplicate. The initially determined $K_{dapp}$ of the APP-E2–Cu complex had to be corrected for competition with the copper ligand Tris and its pH-dependent protonation.[26] The corrected $K_d$ was calculated according to $K_d = K_{dapp}\left(1 + c_{Tris} \times 10^{pK_1(Tris)} / \left(1 + 10^{-pH} \times K_a\right)\right)^{-1}$ using $pK_{1(Tris)} = 3.82$[60] and $pK_{a(Tris)} = 8.1$. In the case of zinc binding, the enthalpic data were fitted to a binding model representing two sets of independent binding sites, accounting for 1 strong

binding site and 3.3 weak binding sites (4.3 total $Zn^{2+}$ sites) per protein molecule. Since $K_{d2}$ is determined not statistically significant in the fit, a $K_{d1}$ of 3.9 μM and a $K_{d2}$ of 2.6 mM have to be regarded as upper (weakest) limits (Table 3). A possibly lower $K_{d2}$ necessarily results in a decreased $K_{d1}$ value. Higher values of $K_{d2}$, however, would affect $K_{d1}$ slightly but would cause an increase in $\Delta H_2$ to values even higher than 1200 kJ/mol, unlikely for non-covalent interactions.

### ITC measurements at high Zn/protein ratios

The effect of excessive zinc-to-protein ratios was studied in ITC experiments, where three repeating titrations were performed in series into the same cell solution. Titration was performed in 20 mM Hepes/NaOH (pH 7.3) and 150 mM NaCl at 20 °C, adding a 0.8 mM $ZnCl_2$ solution in 3 × 22 injections to 40 μM APP-E2, resulting in a final $Zn^{2+}$/protein ratio of 22. The molar ratios for titration experiments 2 and 3 were calculated neglecting intermixture of cell volume and slight volume changes occurring after refill of the syringe. Blank heats for titrations of metals in buffer were subtracted from peak integrals.

### Determination of total $Zn^{2+}$ binding sites on APP-E2

The protein was saturated with 10 mM $ZnCl_2$ in 20 mM Hepes/NaOH (pH 7.3) and 150 mM NaCl, resulting in quantitative precipitation of the protein. The precipitate was washed with buffer until a stable equilibrium ratio of zinc-saturated protein in the liquid phase and the solid phase was reached. The concentrations of $Zn^{2+}$[59] and protein[61] were determined after each wash step in the liquid phase (supernatant) after 5 min of centrifugation at 16,000*g*. The ratio between [$Zn^{2+}$] and [APP-E2] under equilibrium conditions corresponds to the total number of zinc binding sites per protein molecule, which was determined to be 4.3 ± 0.2 (Fig. 3f). Subtraction of the one strong binding site yields the number additional weak binding sites as 3.3.

### SPR analysis

SPR analysis was performed using a BIAcore 3000 setup (GE Healthcare) with an SCB CMD500L sensor chip (Xantec). APP-E2 was coupled to the sensor chip surface *via* an amine coupling protocol according to the manufacturer's instructions in amounts that yielded 6000 RU. Metal binding analysis was performed at 25 °C in 10 mM Hepes, 135 mM NaCl, 6 mM KCl and 5.5 mM glucose at pH 7.1. For metal chelation experiments, 20 mM citrate (Zn) and 20 mM Tris (Cu) at pH 6.8, respectively, were added and injected with a flow rate of 30 μl/min followed by a dissociation phase of 7 min. The chip was rinsed by sequent injections of running buffer containing 3 mM ethylenediaminetetraacetic acid and 10 mM HCl. Spectra were baseline corrected against an unloaded flow cell and set to zero.

### Limited proteolysis

Limited proteolysis was performed in 20 mM Hepes and 150 mM NaCl at pH 7.4 containing 0.5 μg/ml trypsin (Calbiochem) and 20 μM purified protein (α-casein as control). Copper or zinc was supplemented at 40 μM to the samples. Reactions were stopped after 30 and 60 min by addition of 10 mM PMSF and analyzed by SDS-PAGE. Protease cleavage sites were characterized by Edman sequencing (Procise 494A; Applied Biosystems, Foster City, CA, USA). Limited proteolysis experiments were reproduced in three independent experiments.

### CD spectroscopy

CD data were collected on a J-710 spectropolarimeter (Jasco Corporation) employing the ITC-buffers adding 7.5 μM APP-E2 and 10 μM zinc or copper. CD signals were measured at 222 nm upon heating (1 °C/min) of the samples from 20 °C to 90 °C. The blank signals produced by the buffers at 20 °C were subtracted as constant values from the melting curves. Melting points correspond to the maximum of the first-order derivative of the melting curves calculated with spectra analysis software (Jasco Corporation).

### Accession codes

Data deposition: The atomic coordinates and structure factors have been deposited in the PDB‡ (PDB IDs: 3UMH, 3UMI and 3UMK).

## Acknowledgements

The authors thank J. Roy for the help during crystallization and C. Breithaupt for critical reading of the manuscript. We acknowledge the Helmholtz Zentrum Berlin BESSY II for provision of synchrotron radiation at beamlines BL 14.1 and BL 14.2 and thank the scientific staff for assistance. This work was supported by the Deutsche Forschungsgemeinschaft (MU901), the International Copper Association (to G.M.) and the Breuer Stiftung (to G.M.).

## Supplementary Data

Supplementary data associated with this article can be found, in the online version, at doi:10.1016/j.jmb.2011.12.057

## References

1. Blennow, K., de Leon, M. J. & Zetterberg, H. (2006). Alzheimer's disease. *Lancet*, **368**, 387–403.
2. Haass, C. & Selkoe, D. J. (2007). Soluble protein oligomers in neurodegeneration: lessons from the

‡ www.rcsb.org

Alzheimer's amyloid beta-peptide. *Nat. Rev., Mol. Cell Biol.* **8**, 101–112.
3. Lichtenthaler, S. F., Haass, C. & Steiner, H. (2011). Regulated intramembrane proteolysis—lessons from amyloid precursor protein processing. *J. Neurochem.* **117**, 779–796
4. Hung, Y. H., Bush, A. I. & Cherny, R. A. (2010). Copper in the brain and Alzheimer's disease. *J. Biol. Inorg. Chem.* **15**, 61–76.
5. Watt, N. T., Whitehouse, I. J. & Hooper, N. M. (2010). The role of zinc in Alzheimer's disease. *Int. J. Alzheimers Dis.* **2011**, 971021.
6. Bayer, T. A. & Multhaup, G. (2006). The role of metal ions in the amyloid precursor protein and in Alzheimer's disease. In *Neurodegenerative Diseases and Metal Ions* (Sigel, A., Sigel, H. & Sigel, R. K. O., eds), Vol. 1, John Wiley & Sons, Ltd, Chichester, UK.
7. Jacobsen, K. T. & Iverfeldt, K. (2009). Amyloid precursor protein and its homologues: a family of proteolysis-dependent receptors. *Cell. Mol. Life Sci.* **66**, 2299–2318.
8. Dahms, S. O., Hoefgen, S., Roeser, D., Schlott, B., Guhrs, K. H. & Than, M. E. (2010). Structure and biochemical analysis of the heparin-induced E1 dimer of the amyloid precursor protein. *Proc. Natl Acad. Sci. USA*, **107**, 5381–5386.
9. Reinhard, C., Hebert, S. S. & De Strooper, B. (2005). The amyloid-beta precursor protein: integrating structure with biological function. *EMBO J.* **24**, 3996–4006.
10. Soba, P., Eggert, S., Wagner, K., Zentgraf, H., Siehl, K., Kreger, S. *et al.* (2005). Homo- and heterodimerization of APP family members promotes intercellular adhesion. *EMBO J.* **24**, 3624–3634.
11. Kaden, D., Munter, L. M., Joshi, M., Treiber, C., Weise, C., Bethge, T. *et al.* (2008). Homophilic interactions of the amyloid precursor protein (APP) ectodomain are regulated by the loop region and affect beta-secretase cleavage of APP. *J. Biol. Chem.* **283**, 7271–7279.
12. Scheuermann, S., Hambsch, B., Hesse, L., Stumm, J., Schmidt, C., Beher, D. *et al.* (2001). Homodimerization of amyloid precursor protein and its implication in the amyloidogenic pathway of Alzheimer's disease. *J. Biol. Chem.* **276**, 33923–33929.
13. Gralle, M., Oliveira, C. L., Guerreiro, L. H., McKinstry, W. J., Galatis, D., Masters, C. L. *et al.* (2006). Solution conformation and heparin-induced dimerization of the full-length extracellular domain of the human amyloid precursor protein. *J. Mol. Biol.* **357**, 493–508.
14. Wang, Y. & Ha, Y. (2004). The X-ray structure of an antiparallel dimer of the human amyloid precursor protein E2 domain. *Mol. Cell*, **15**, 343–353.
15. Kaden, D., Voigt, P., Munter, L. M., Bobowski, K. D., Schaefer, M. & Multhaup, G. (2009). Subcellular localization and dimerization of APLP1 are strikingly different from APP and APLP2. *J. Cell Sci.* **122**, 368–377.
16. Lee, S., Xue, Y., Hu, J., Wang, Y., Liu, X., Demeler, B. & Ha, Y. (2011). The E2 domains of APP and APLP1 share a conserved mode of dimerization. *Biochemistry*, **50**, 5453–5464.
17. Baumkotter, F., Wagner, K., Eggert, S., Wild, K. & Kins, S. (2011). Structural aspects and physiological consequences of APP/APLP trans-dimerization. *Exp. Brain Res.* Sep 28. [Epub ahead of print], doi:10.1007/s00221-011-2878-6.
18. Xue, Y., Lee, S. & Ha, Y. (2011). Crystal structure of amyloid precursor-like protein 1 and heparin complex suggests a dual role of heparin in E2 dimerization. *Proc. Natl Acad. Sci. USA*, **108**, 16229–16234.
19. Keil, C., Huber, R., Bode, W. & Than, M. E. (2004). Cloning, expression, crystallization and initial crystallographic analysis of the C-terminal domain of the amyloid precursor protein APP. *Acta Crystallogr., Sect. D: Biol. Crystallogr.* **60**, 1614–1617.
20. Hoopes, J. T., Liu, X., Xu, X., Demeler, B., Folta-Stogniew, E., Li, C. & Ha, Y. (2010). Structural characterization of the E2 domain of APL-1, a *Caenorhabditis elegans* homolog of human amyloid precursor protein, and its heparin binding site. *J. Biol. Chem.* **285**, 2165–2173.
21. Dulubova, I., Ho, A., Huryeva, I., Sudhof, T. C. & Rizo, J. (2004). Three-dimensional structure of an independently folded extracellular domain of human amyloid-beta precursor protein. *Biochemistry*, **43**, 9583–9588.
22. Hesse, L., Beher, D., Masters, C. L. & Multhaup, G. (1994). The beta A4 amyloid precursor protein binding to copper. *FEBS Lett.* **349**, 109–116.
23. Bush, A. I., Multhaup, G., Moir, R. D., Williamson, T. G., Small, D. H., Rumble, B. *et al.* (1993). A novel zinc(II) binding site modulates the function of the beta A4 amyloid protein precursor of Alzheimer's disease. *J. Biol. Chem.* **268**, 16109–16112.
24. Kong, G. K., Adams, J. J., Harris, H. H., Boas, J. F., Curtain, C. C., Galatis, D. *et al.* (2007). Structural studies of the Alzheimer's amyloid precursor protein copper-binding domain reveal how it binds copper ions. *J. Mol. Biol.* **367**, 148–161.
25. Than, M. E., Henrich, S., Bourenkov, G. P., Bartunik, H. D., Huber, R. & Bode, W. (2005). The endoproteinase furin contains two essential $Ca^{2+}$ ions stabilizing its N-terminus and the unique S1 specificity pocket. *Acta Crystallogr., Sect. D: Biol. Crystallogr.* **61**, 505–512.
26. Hatcher, L. Q., Hong, L., Bush, W. D., Carducci, T. & Simon, J. D. (2008). Quantification of the binding constant of copper(II) to the amyloid-beta peptide. *J. Phys. Chem. B*, **112**, 8160–8164.
27. Jefferson, T., Causevic, M., auf dem Keller, U., Schilling, O., Isbert, S., Geyer, R. *et al.* (2011). Metalloprotease meprin beta generates nontoxic N-terminal amyloid precursor protein fragments *in vivo*. *J. Biol. Chem.* **286**, 27741–27750.
28. Harding, M. M. (2004). The architecture of metal coordination groups in proteins. *Acta Crystallogr., Sect. D: Biol. Crystallogr.* **60**, 849–859.
29. Han, Q., Fu, Y., Zhou, H., He, Y. & Luo, Y. (2007). Contributions of Zn(II)-binding to the structural stability of endostatin. *FEBS Lett.* **581**, 3027–3032.
30. Gifford, J. L., Walsh, M. P. & Vogel, H. J. (2007). Structures and metal-ion-binding properties of the $Ca^{2+}$-binding helix–loop–helix EF-hand motifs. *Biochem. J.* **405**, 199–221.
31. Schubert, W., Prior, R., Weidemann, A., Dircksen, H., Multhaup, G., Masters, C. L. & Beyreuther, K. (1991). Localization of Alzheimer beta A4 amyloid precursor protein at central and peripheral synaptic sites. *Brain Res.* **563**, 184–194.

32. Sabo, S. L., Ikin, A. F., Buxbaum, J. D. & Greengard, P. (2003). The amyloid precursor protein and its regulatory protein, FE65, in growth cones and synapses *in vitro* and *in vivo*. *J. Neurosci.* **23**, 5407–5415.
33. Groemer, T. W., Thiel, C. S., Holt, M., Riedel, D., Hua, Y., Huve, J. *et al.* (2011). Amyloid precursor protein is trafficked and secreted *via* synaptic vesicles. *PLoS One*, **6**, e18754.
34. Paoletti, P., Vergnano, A. M., Barbour, B. & Casado, M. (2009). Zinc at glutamatergic synapses. *Neuroscience*, **158**, 126–136.
35. Frederickson, C. J., Giblin, L. J., 3rd, Balaji, R. V., Masalha, R., Frederickson, C. J., Zeng, Y. *et al.* (2006). Synaptic release of zinc from brain slices: factors governing release, imaging, and accurate calculation of concentration. *J. Neurosci. Methods*, **154**, 19–29.
36. Boll, M. C., Alcaraz-Zubeldia, M., Montes, S. & Rios, C. (2008). Free copper, ferroxidase and SOD1 activities, lipid peroxidation and NO(x) content in the CSF. A different marker profile in four neurodegenerative diseases. *Neurochem. Res.* **33**, 1717–1723.
37. Anliker, B. & Muller, U. (2006). The functions of mammalian amyloid precursor protein and related amyloid precursor-like proteins. *Neurodegener. Dis.* **3**, 239–246.
38. Duce, J. A., Tsatsanis, A., Cater, M. A., James, S. A., Robb, E., Wikhe, K. *et al.* (2010). Iron-export ferroxidase activity of beta-amyloid precursor protein is inhibited by zinc in Alzheimer's disease. *Cell*, **142**, 857–867.
39. Goodman, Y. & Mattson, M. P. (1994). Secreted forms of beta-amyloid precursor protein protect hippocampal neurons against amyloid beta-peptide-induced oxidative injury. *Exp. Neurol.* **128**, 1–12.
40. Clement, A. B., Gimpl, G. & Behl, C. (2010). Oxidative stress resistance in hippocampal cells is associated with altered membrane fluidity and enhanced nonamyloidogenic cleavage of endogenous amyloid precursor protein. *Free Radical Biol. Med.* **48**, 1236–1241.
41. Lezoualc'h, F., Engert, S., Berning, B. & Behl, C. (2000). Corticotropin-releasing hormone-mediated neuroprotection against oxidative stress is associated with the increased release of non-amyloidogenic amyloid beta precursor protein and with the suppression of nuclear factor-kappaB. *Mol. Endocrinol.* **14**, 147–159.
42. Ho, A. & Sudhof, T. C. (2004). Binding of F-spondin to amyloid-beta precursor protein: a candidate amyloid-beta precursor protein ligand that modulates amyloid-beta precursor protein cleavage. *Proc. Natl Acad. Sci. USA*, **101**, 2548–2553.
43. Hoe, H. S., Wessner, D., Beffert, U., Becker, A. G., Matsuoka, Y. & Rebeck, G. W. (2005). F-spondin interaction with the apolipoprotein E receptor ApoEr2 affects processing of amyloid precursor protein. *Mol. Cell Biol.* **25**, 9259–9268.
44. Andersen, O. M., Schmidt, V., Spoelgen, R., Gliemann, J., Behlke, J., Galatis, D. *et al.* (2006). Molecular dissection of the interaction between amyloid precursor protein and its neuronal trafficking receptor SorLA/LR11. *Biochemistry*, **45**, 2618–2628.
45. Acevedo, K. M., Hung, Y. H., Dalziel, A. H., Li, Q. X., Laughton, K., Wikhe, K. *et al.* (2011). Copper promotes the trafficking of the amyloid precursor protein. *J. Biol. Chem.* **286**, 8252–8262.
46. Hung, Y. H., Robb, E. L., Volitakis, I., Ho, M., Evin, G., Li, Q. X. *et al.* (2009). Paradoxical condensation of copper with elevated beta-amyloid in lipid rafts under cellular copper deficiency conditions: implications for Alzheimer disease. *J. Biol. Chem.* **284**, 21899–21907.
47. Collaborative Computational Project. (1994). The CCP4 suite: programs for protein crystallography. *Acta Crystallogr., Sect. D: Biol. Crystallogr.* **50**, 760–763.
48. Stein, N. (2008). CHAINSAW: a program for mutating pdb files used as templates in molecular replacement. *J. Appl. Crystallogr.* **41**, 641–643.
49. McCoy, A. J., Grosse-Kunstleve, R. W., Adams, P. D., Winn, M. D., Storoni, L. C. & Read, R. J. (2007). Phaser crystallographic software. *J. Appl. Crystallogr.* **40**, 658–674.
50. de La Fortelle, E. & Bricogne, G. (1997). Maximum-likelihood heavy-atom parameter refinement for multiple isomorphous replacement and multiwavelength anomalous diffraction methods. *Methods Enzymol.* **276**, 472–494.
51. Cowtan, K. (2006). The Buccaneer software for automated model building. 1. Tracing protein chains. *Acta Crystallogr., Sect. D: Biol. Crystallogr.* **62**, 1002–1011.
52. Turk, D. (1992). Weiterentwicklung eines Programms für Molekülgraphik und Elektronendichte-Manipulation und seine Anwendung auf verschiedene Protein Strukturaufklärungen. PhD thesis (Technische Universität München, Munich, Germany).
53. Brunger, A. T. (2007). Version 1.2 of the crystallography and NMR system. *Nat. Protoc.* **2**, 2728–2733.
54. Ramachandran, G. N. & Sasisekharan, V. (1968). Conformation of polypeptides and proteins. *Adv. Protein Chem.* **23**, 283–438.
55. Allen, F. H. (2002). The Cambridge Structural Database: a quarter of a million crystal structures and rising. *Acta Crystallogr., Sect. B: Struct. Sci.* **58**, 380–388.
56. Krissinel, E. & Henrick, K. (2007). Inference of macromolecular assemblies from crystalline state. *J. Mol. Biol.* **372**, 774–797.
57. Edgar, R. C. (2004). MUSCLE: multiple sequence alignment with high accuracy and high throughput. *Nucleic Acids Res.* **32**, 1792–1797.
58. UniProt (2011). Ongoing and future developments at the Universal Protein Resource. *Nucleic Acids Res.* **39**, D214–D219.
59. Sabel, C. E., Neureuther, J. M. & Siemann, S. (2010). A spectrophotometric method for the determination of zinc, copper, and cobalt ions in metalloproteins using Zincon. *Anal. Biochem.* **397**, 218–226.
60. Canepari, S., Carunchio, V., Castellano, P. & Messina, A. (1999). Complex formation equilibria of some beta-amino-alcohols with lead(II) and cadmium(II) in aqueous solution. *Talanta*, **47**, 1077–1084.
61. Bradford, M. M. (1976). A rapid and sensitive method for the quantitation of microgram quantities of protein utilizing the principle of protein–dye binding. *Anal. Biochem.* **72**, 248–254.